Analytical Biochemistry 531 (2017) 48–55

Contents lists available at ScienceDirect

Analytical Biochemistry

journal homepage: www.elsevier.com/locate/yabio

Dopamine modified hyperbranched TiO_2 arrays based ultrasensitive photoelectrochemical immunosensor for detecting neuron specific enolase

He Li*, Qiyou Xiao, Jiaxin Lv, Qin Lei, Yujie Huang

School of Chemistry and Environment, South China Normal University, Guangzhou Key Laboratory of Analytical Chemistry for Biomedicine, Guangzhou 510006, China

ARTICLE INFO

Article history:
Received 14 January 2017
Received in revised form
20 May 2017
Accepted 24 May 2017
Available online 25 May 2017

Keywords:
Photoelectrochemical immunosensor
Neuron specific enolase
Small-cell lung carcinoma (SCLC)
Hyperbranched titanium dioxide

ABSTRACT

In this work, three-dimensional (3D) hyperbranched TiO_2 nanorod arrays were synthesized and used to fabricate dopamine sensitized photoelectrochemical (PEC) biosensor. To increase the lifetime of charge carriers and enhance the photocurrent responses signal, a delicate signal amplification strategy by introducing dopamine (DA) as sensitizer was developed. The dopamine sensitized TiO_2 can shorten the carrier diffusion distance, improve light harvesting efficiency and charge collection efficiency, which results in performance improvement of the as-obtained PEC sensor. This proposed biosensor for determination of neuron specific enolase (NSE) demonstrated a good linear relationship range from 0.1 ng mL^{-1} to 1000 ng mL^{-1} with a detection limit of 0.05 $ngmL^{-1}$ (S/N = 3). In addition, the as-prepared immunosensor exhibits excellent selectivity, stability and reproducibility, which could be extended to other label-free sensing fields. Therefore, this proposed method may also provide potential applications for the clinical examination.

Introduction

Accurate and sensitive determination of disease-related biomarkers is very significant to diagnosis and therapy of disease [1]. What' more, the precise detection of tumor biomarkers exhibits great promise for advanced prediction and early diagnosis [2]. Lung cancer is the leading cause of cancer mortality worldwide. Neuron specific enolase (NSE) is a reliable, specific and sensitive tumor marker for small-cell lung carcinoma (SCLC). For the healthy people, NSE levels are 5–12 $ngmL^{-1}$ in serum and <20 $ngmL^{-1}$ in cerebrospinal fluid [3]. If the people suffer from lung cancer, the NSE level in blood will change. Therefore, it is of great significance to monitor NSE for routine examination, diagnosis and therapy of SCLC. Up to now, a lot of analytical methods have been developed for NSE determination, such as fluoroimmunoassay [4], radioimmunoassay [5], enzyme-linked immunosorbent assay [6], chemiluminescence immunoassay [7] and electrochemical immunoassay [8]. Each analytical method has its own merit and limitation. For example, electrochemical method was simple, rapid and highly sensitive. Developing simple, highly sensitive, stable and inexpensive methods to determine NSE were very important for both healthy people and cancer patients.

PEC immunosensing is a promising method for high throughput and rapid bioanalysis [9]. Many photoelectrochemical active nanomaterials such as CdSe [10], ZnO [11] and TiO_2 [12] have obtained great attention for fabrication of biosensors. Particularly, as an outstanding electrode material in PEC biosensor, TiO_2 has been proved to be good biocompatibility, environmental safety and inexpensiveness [13–15]. Nevertheless, pristine TiO_2 still has some shortcomings for application in bioanalysis, such as low utilization efficiency of solar light and biomolecule damage under ultraviolet light irradiation. How to overcome these defects and expand its application is still a great challenge [16–19].

In order to improve the electrochemical and PEC performance of TiO_2, we try to enhance its photocurrent by doping heteroatom in TiO_2 structure [20,21]. In addition, other materials (such as quantum dot and graphene) modified TiO_2 have also been reported [22–24]. The proposed PEC immunosensor fully utilized the advantages of both the high selectivity due to the specific interaction between antibody and antigen and the signal amplification strategy of dopamine sensitized PEC sensor. It was conducive to improve

* Corresponding author.
E-mail address: analchemlh@163.com (H. Li).

http://dx.doi.org/10.1016/j.ab.2017.05.025
0003-2697/

sensitivity and selectivity of this proposed immunoassay.

Materials and methods

Chemicals

Potassium titanyl oxalate ($K_2TiO \cdot C_4O_8$) and titanium trichloride ($TiCl_3$) were purchased from McLean Biochemical Technology Co., LTD (Shanghai, China). Ascorbic acid (AA), glutaraldehyde (GD) and Bovine serum albumin (BSA) were bought from Aladdin Reagent Company (Shanghai, China). NSE, rabbit antihuman neuron specific enolase (anti-NSE), carcinoembryonic antigen (CEA), prostate specific antigen (PSA), immunoglobulin G (IgG), α-fetoprotein (AFP) and Cytokeratin 19 fragment antigen 21-1 (CYFRA21-1) were purchased from Beijing Biosynthesis Biotechnology Co., LTD (Beijing, China). Fluorine-doped tin oxide (FTO) was obtained from Zhuhai Kaivo Optoelectronic Technology Co., Ltd (Zhuhai, China). The buffer solution was consist of phosphate buffer solution (0.1 M, pH = 7.4). Human serum samples were achieved from Zhujiang Hospital of Southern Medical University. Other reagents were all analytical grade and provided by Guangzhou Chemical Reagent Factory (Guangzhou, China).

Apparatus

All electrochemical determination was carried out on an Autolab electrochemical workstation (PGSTAT302N, Metrohm, Switzerland). A three-electrode system was composed of a platinum column counter electrode, the modified FTO working electrode (0.64 cm^2) and Ag/AgCl reference electrode. Electrochemical impedance spectroscopy (EIS) was carried out in KCl solution (0.1 M) containing $K_3[Fe(CN)_6]/K_4[Fe(CN)_6]$ (5 mM, 1:1) mixture as a redox probe, and conducted at an open circuit potential of 0.22 V over a frequency range of 10^{-2} Hz- 10^5 Hz, with an amplitude of 5 mV. All the photocurrent measurements were performed at a constant potential of 0 V (vs saturated Ag/AgCl electrode) in 0.1 M PBS (pH 7.4) containing 50 mM AA. The light source was purchused from Guangzhou Hiclean Chemical Co., Ltd. The LED lamp (3 W) with specified wavelength was used as irradiation source. The light was regularly switched on and off for 20 s, respectively. X-ray diffraction (XRD) was performed on Bruker D8 advance X-ray diffractometer with Cu K_α radiation ($\lambda = 0.1542$ nm) (Bruker, Germany). The 2θ range used in the measurements was from 20° to 80°. Zeiss Ultra55 field emission scanning electronmicroscope (Carl Zeiss, Germany) was employed for scanning electron micrographs (SEM).

Preparation of 3D hyperbranched TiO_2 nanorod arrays

3D hyperbranched TiO_2 nanorod arrays were synthesized according to a previous report with some modifications [25]. In detail, TiO_2 nanorods (NRs) were prepared on FTO substrates via a solvothermal method. FTO substrates (0.8 × 0.8 cm), cleaned by acetone, ethanol and deionized (DI) water, were immersed in the mixed solution consisted of potassium titanyl oxalate, DI water and hydrochloric acid at 150°Cfor 6 h. Afterwards, the branched TiO_2 NRs were obtained by a two-step procedure. At first, the as-prepared NRs were immersed in a high concentration of potassium titanyl oxalate aqueous solution and kept at 100°Cfor 1 h to selective germination and attachment. Then, these seeded NRs were transferred into the same solution which as described in the preparation of NRs section for further reaction 3 h to synthesized TiO_2 HNRs. The preparation of 3D hyperbranched TiO_2 nanorods (HHNRs) was as follows: Firstly, to obtain the densely packed hyperbranched nanostructure, HNRs were calcined at 450°Cfor 30 min. Afterwards, it was put in a mixed aqueous solution which consisted of DI water, titanium trichloride and hydrochloric acid at 80 °C to react for 2 h. Eventually, it was calcined at 450°Cfor 30 min in air.

Fabrication of PEC immunosensor

Dopamine sensitized TiO_2 (FTO/TiO_2/DA) electrodes were fabricated by immersing HHNRs modified electrodes in a freshly prepared dopamine aqueous solution (0.015 M) for 15 min. Next, the DA modified electrodes were rinsed with buffer solution before use. The procedure of fabricating PEC was shown in Fig. 1. The immobilization of NSE antibodies (anti-NSE) onto DA/TiO_2/FTO electrodes can be realized through the covalent cross-linking reaction between amino groups and aldehyde groups. Firstly, the modified electrodes were dipped into glutaraldehyde solution (GD 5%) for 30 min to activate the -NH_2 group in DA. Subsequently, the FTO/TiO_2/DA/GD-activated electrodes were incubated in anti-NSE (50 $\mu g mL^{-1}$) solution at 4°Cfor 12 h to immobilize anti-NSE. Then, the electrodes were incubated in BSA solution (1%, w/w) for 1 h to block remaining sites and avoid nonspecific binding to obtain anti-NSE/DA/TiO_2/FTO sensing platform. Ultimately, the achieved immunosensor was washed with PBS buffer solution for several times and was stored at 4 °C when it was not in use.

Results and discussion

Characterization of TiO_2

The morphologies of as-synthesized TiO_2 were characterized by SEM and shown in Fig. 2. Fig. 2B, D and 2F exhibited that the diameter of the nanorods did not significantly change even after branched (Fig. 2D) and hyperbranched (Fig. 2F) treatment, which reveal a similar value of approximately 50 nm. Fig. 2A showed that the NRs scaffolds were relatively smooth, which had been proven to be available for the rapid electron transport, but the improvement of photoelectric performance was limited by the low specific surface area when applied in PEC biosensors [26]. Subsequently, HNRs epitaxially germinated on the backbone of NRs through a secondary solvothermal method, a hierarchical branched nanorod architecture was formed (Fig. 2C). This could be attributed to the selective germination and adsorption, which would minimize the total free energy during the nucleation and crystallization process [27]. Ultimately, there were many nanorods (about 50 nm in length and 20 nm in thickness) were grown on the HNRs backbone. The originally branched structures were changed obviously into hyperbranched features with a higher branched level (Fig. 2F and E). Such extremely branched 3D nanostructure was believed to enhance not only the light absorption ability but also the photocurrent response, which brought about the improvement of photoelectric performance of the PEC biosensors. According to the energy dispersed spectrum (EDS) measurement (Supporting information Fig. S1), the existence of Ti, O and Sn elements in the as-synthesized electrodes was confirmed. While Sn element was derived from SnO_2 existing in the FTO glass and the other peaks corresponded to the diffraction peak of Pt elements, which was coated on the surface of as-obtained TiO_2 samples during the process of characterization.

XRD was employed to characterize structure information of the as-obtained TiO_2. Fig. 3A exhibited XRD patterns of TiO_2 NRs, HNRs and HHNRs grown on FTO substrates, respectively. The main diffraction peaks of synthesized TiO_2 can be indexed to the rutile phase (JCPDS, 21-1276), which suggested that the rutile phase TiO_2 was individually formed during the process of solvothermal treatment. The enhanced diffraction peak at 2θ = 36.09° corresponded

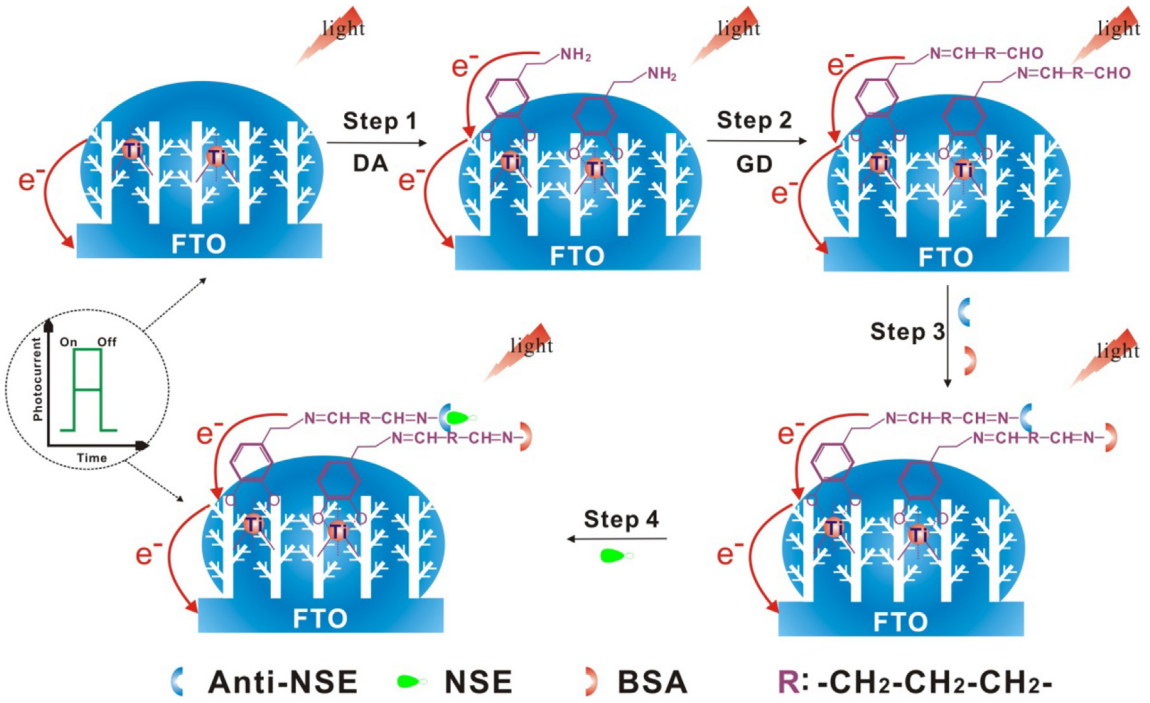

Fig. 1. Schematic diagram of photoelectrochemical immunosensor.

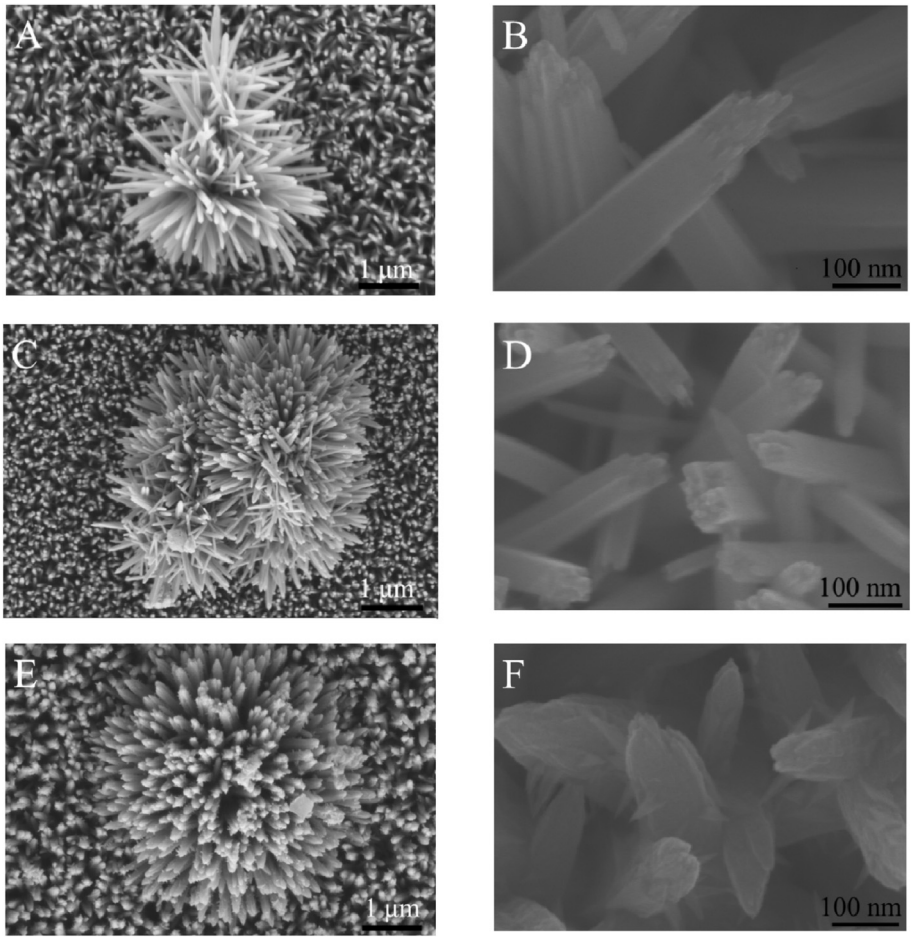

Fig. 2. SEM images of TiO_2 NRs (1A and 1B), HNRs (1C and 1D) and HHNRs (1E and 1F).

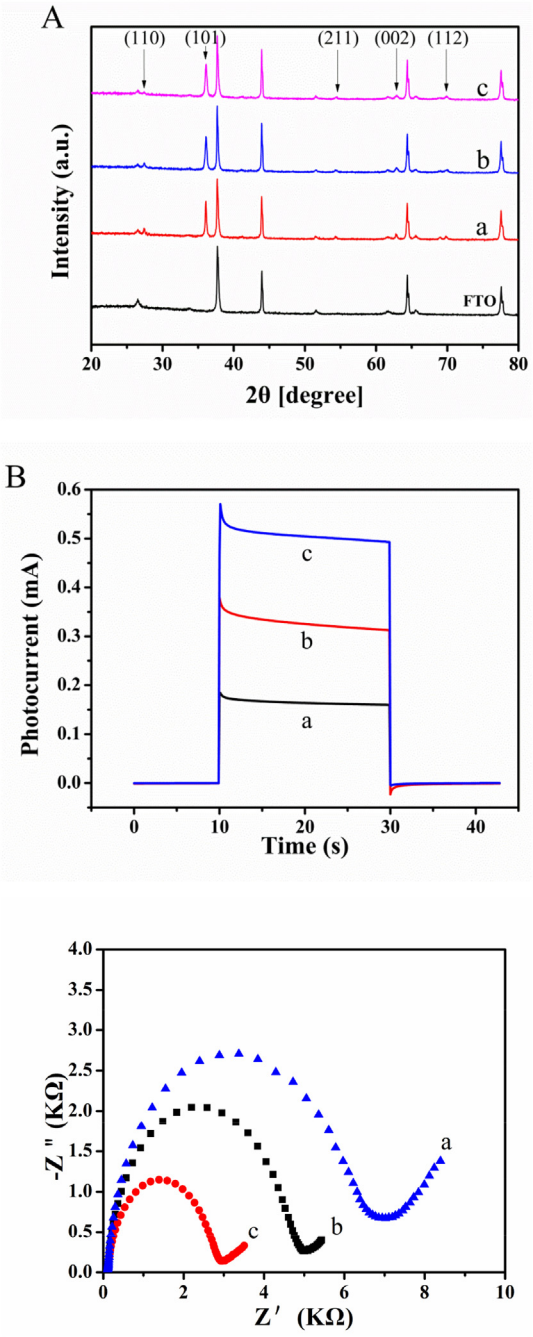

Fig. 3. XRD patterns (A), photocurrent responses (B) and EIS (C) of TiO_2 NRs(a), HNRs(b) and HHNRs(c). XRD was performed on a D8 Advance X-ray diffractometer with Cu K_α radiation ($\lambda = 0.1542$ nm), and recorded for 2θ angles between 20° and 80°; photocurrent measurements were performed at a constant potential of 0 V (vs saturated Ag/AgCl electrode) in 0.1 M PBS (pH 7.4) containing 50 mM AA; EIS was carried out in KCl solution (0.1 M) containing $K_3[Fe(CN)_6]/K_4[Fe(CN)_6]$ (5 mM, 1:1) mixture as a redox probe, and conducted at an open circuit potential of 0.22 V over a frequency range of 10^{-2} Hz- 10^5 Hz, with an amplitude of 5 mV.

to the (101) lattice planes, the narrow sharp diffraction peaks at 2θ = 27.43°, 54.44°, 62.84° and 69.81° corresponded to the (110), (211), (002) and (112) lattice planes, respectively. The peak intensity of (110) became weak in the XRD patterns of HNRs and HHNRs, which could be explained by the fact that the substrate NRs were attached by branched and hyperbranched NRs [25]. While the other unmarked peaks corresponded to the diffraction peak of SnO_2 existing in the FTO glass, which indicated no other impurities appeared in the as-prepared TiO_2. The stability of active photoelectric material was investigated during PEC preparing process. The photocurrent response of NRs, HNRs, and HHNRs modified electrodes were relatively stable, at a bias potential of 0 V vs. RHE, as displayed in Fig. 3B. It can be seen that the NRs, HNRs and HHNRs have rapid photo-response time and superior photo-stability, which demonstrated the good characteristic of the TiO_2 crystal structures.

To further research the dynamic process of charge transport and recombination of NRs, HNRs and HHNRs modified electrodes, EIS were carried out and illustrated in Fig. 3C. Typically, semicircle reveals the recombination resistance for the electron transfer process between electrolyte interface and the semiconductor array. In particular, along with the increase of the degree of branching, the electron transfer pathway was shortened in HNRs and became even more easier in HHNRs [27]. Compared with the nanoparticles and nanowires, the 3D hyperbranched nanorods with smooth, hierarchical and hyperbranched structure, had slower recombination rate and longer electron lifetime within PEC sensor [28]. It could be explained by the fact the 3D hyperbranched nanostructure would, to a certain degree, cut down the electron transfer pathway, and the larger surface area of these films would result in fewer grain boundaries and provide fewer recombination centers and trapping sites for more slight recombination within PEC biosensor [27].

Characterization of PEC immunosensor

The anti-NSE/DA/TiO_2/FTO based PEC immunosensor was characterized by EIS. Fig. 4A demonstrated the Nyquist plots of $K_3Fe(CN)_6/K_4Fe(CN)_6$ at different electrodes. The inset is an equivalent circuit. Where, R_s, C_{dl}, R_{ct} and Z_w represent the resistance of electrolyte solution, the double-layer capacitance, charge transfer resistance and Warburg impedance, respectively. The Nyquist plots indicated that the electrode modified with 3D hyperbranched TiO_2 presented a higher charge transfer resistance(R_{ct}), which was fitted to be 6.0 kΩ because of its poor electronic conductivity of TiO_2 (curve a). Obviously, the R_{ct} value decreased significantly to 4.6 kΩ after immersing TiO_2 in dopamine solution for 15 min (curve b), this could be explained by the fact that the enediol-ligands in the structure of DA can bound to the titanium atom of TiO_2 to form TiO_2-DA charge transfer complex [29]. Afterwards, when the anti-NSE was immobilized onto DA/TiO_2/FTO electrodes surface (curve c), the value of Rct increased to 5.4 kΩ. With the nonspecific binding sites were blocked through BSA (curve d), the R_{ct} continuously increased to 6.6 kΩ. It could be attributed to the fact that the biomacromolecule immobilized on the electrode would hinder electron transfer between the redox probe and the electrode surface. In the same way, it was found that the R_{ct} has been increased further to 7.9 kΩ after the specific interaction between NSE and anti-NSE (curve e), which was ascribed to the increase of steric hindrance effect.

To characterize the fabrication process of anti-NSE/DA/TiO_2/FTO electrode, we also surveyed the photocurrent response of the proposed PEC immunosensor in 50 mM AA (as an electron donor), which could scavenge the photo-generated holes of TiO_2 and hinder the processes of electron-hole recombination, thus increase the photocurrent response. As shown in Fig. 4B, TiO_2/FTO (curve a) showed a high sensitive PEC response because of its large specific surface area, which was beneficial to the effective interfacial charge transfer, enhanced light-harvesting ability and rapid electrolyte diffusion. Subsequently, DA/TiO_2/FTO (curve b) displayed significant increase in photocurrent response, this could be ascribed to the fact that, a transient electron transfer was achieved from the chelate directly into the conduction band (CB) of TiO_2 under light

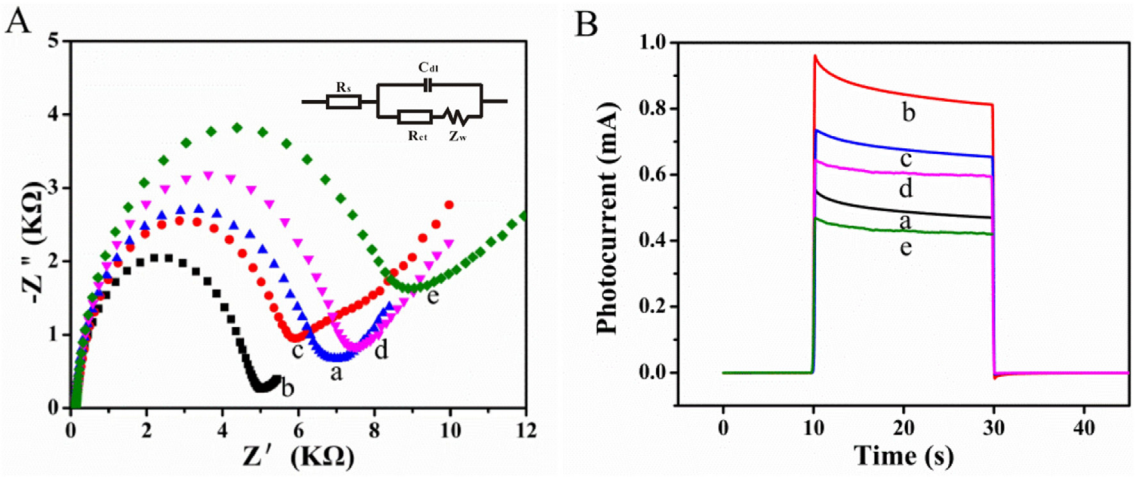

Fig. 4. Electrochemical impendence spectroscopy (A) and photocurrent response (B) of TiO_2(a); Dopamine decoration (b); anti-NSE immobilization (c); blocking with BSA (d); and being incubated in NSE solution at the concentration of 1.0 ng/mL (e). EIS was carried out in KCl solution (0.1 M) containing $K_3[Fe(CN)_6]/K_4[Fe(CN)_6]$ (5 mM, 1:1) mixture as a redox probe, and conducted at an open circuit potential of 0.22 V over a frequency range of 10^{-2} Hz- 10^5 Hz, with an amplitude of 5 mV. Photocurrent measurements were performed at a constant potential of 0 V (vs saturated Ag/AgCl electrode) in 0.1 M PBS (pH 7.4) containing 50 mM AA.

irradiation [30]. It was found that the value of photocurrent response gradually decreased after the DA/TiO_2/FTO electrode combine with anti-NSE (curve c) and BSA (curve d), respectively. It could be attributed to the fact that proteins assembled on to the DA/TiO_2/FTO electrode would block the removal of AA to DA/TiO_2/FTO. Therefore, these reasons resulted in hindering the reaction between photogenerated holes with DA and impairing the photocurrent response as well. When the NSE interacted with the anti-NSE (curve e), the photocurrent further decreased. Hence, according to the variation of the photocurrent during the immunoreaction process, the analyte (target compound) could be detected by this proposed PEC immunosensor.

Optimization of experimental conditions

Due to the incubation time and temperature for the antigen-antibody interaction had serious effects on the performance of the as-obtained immunosensor [31]. Fig. 5A displayed the impact of incubation temperature on the photocurrent responses for the detection of NSE, which was measured at different temperatures ranging from 20 °C to 45 °C. Apparently, the photocurrent increased with the increasement of incubation temperature of 20 °C–35 °C, which was owed to the augment of immunoreaction rate between NSE and anti-NSE. Whereas the photocurrent responses decreased when the temperature exceeded 35 °C, this could be explained that high temperature would lead to an irreversible denaturation of NSE. On the other hand, the immunoreaction rate would be attenuated at low temperature so that the incubation time would be extended. As a result, the optimal incubation temperature was 35 °C. As can be seen from Fig. 5B, the value of photocurrent increased gradually with incubation time and trended to balance at 30 min. There was no obvious change in the response of photocurrent when the incubation time was more than 30 min, this could be ascribed to the fact that the equilibrium for immunoreaction has achieved. Therefore, 30 min was employed as incubation time for the following experiments.

To obtain the optimal experimental conditions for determination of NSE, the pH of PBS and excitation wavelength were also investigated. The effect of the pH of PBS was surveyed from 6.0 to 8.5 at an applied potential of 0 V. As shown in Fig. S2 (Supporting information), the value of photocurrent response increased prominently in accord with the increasing pH range from 6.0 to 7.4, after

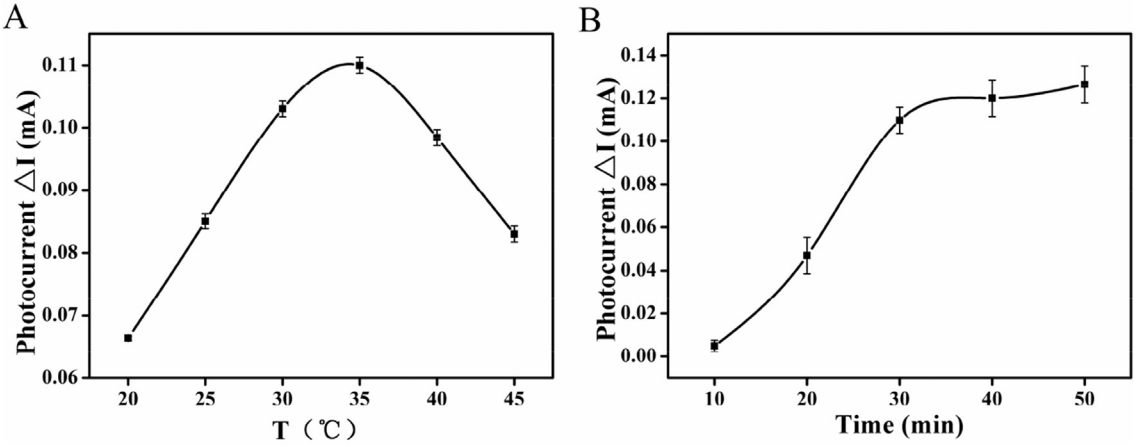

Fig. 5. Effects of incubation temperature (A) and incubation time (B) on photocurrent responses of BSA/anti-NSE/DA/TiO_2/FTO electrode at the presence of 5.0 ng/mL of NSE solution and 0.1 M PBS (pH = 7.4).

that, it reached a platform. Due to the activity of biomolecule would be damaged in the alkaline solution. Therefore, pH = 7.4 was selected for the following experiments. In this work, the constructed PEC immunosensor for NSE determination was based on the UV-visible light excitation. Hence the impacts of irradiation wavelength of 365, 375, 395, 420, 450, 475, 490, 520 and 590 nm on the photocurrent response were also studied, respectively. The results were shown in Fig. S3 (Supporting information), which exhibited that the maximum value of photocurrent response was achieved under 395 nm. Thus, 395 nm was chosen as the optimal excitation wavelength.

Specificity, stability and reproducibility

Specificity is a key factor for immunosensing and nonspecific adsorption is a primary problem in immunoassay [32]. As we know, human serum usually contains many ingredients, such as immunoglobulin G (IgG), prostate-specific antigen (PSA), cytokeratin 19 fragment antigen (CYFRA21-1), carcinoembryonic antigen (CEA) and alpha-fetoprotein (AFP). These components may interfere the detection of NSE by the nonspecific adsorption. For the sake of investigating the specificity of the proposed immunosensor, controllable experiments were employed. The value of photocurrent for the BSA/anti-NSE/DA/TiO_2/FTO electrodes in the presence of 0.1 ng/mL NSE, 1.0 ng/mL IgG, PSA, AFP, CEA and CYFRA21-1 were shown in Fig. 6A. The results indicated that there was no significant influence (SD $\leq$ 9.5%, n = 3) on the determination of NSE, although the concentration of other serum components are 10 times than that of NSE, which suggested that the as-prepared immunosensor possesses an acceptable specificity.

The stability of the as-obtained immunosensor was researched by measuring the photocurrent responses 10 times successively. As presented in Fig. 6B, there were no obvious changes in the photocurrent response was found, indicating a good stability. Furthermore, the long-term stability of the proposed immunosensor was also performed by detecting the value of photocurrent for 1.0 ng mL^{-1} NSE. When it was stored in the refrigerator at 4 °C for two weeks and a month respectively, only a negligible change was found (98.4% and 95.6%) as compared with initial photocurrent response in the determination of 1.0 ng mL^{-1} NSE. Thus, the result illustrated that the proposed immunosensor possess acceptable long-term storage stability.

The reproducibility was performed via measuring 1.0 ng mL^{-1} NSE solution employing five as-prepared immunosensors constructed under the same conditions. The value of RSD for the photocurrent responses was only 2.5%. Therefore, the results illustrated a satisfactory reproducibility of the proposed protocol.

Standard curve of NSE

For the resulted immunoassay, the NSE concentration was linearly correlated to the value of photocurrent. Fig. 7A exhibits the photocurrent response of the proposed immunosensor in the presence of various concentrations of NSE. We can find that the photocurrent responses declined gradually with the increase of NSE concentrations under the optimum conditions. This could be explained by the fact that the formation of immune-complex impeded electron transfer. The change of the photocurrent ($\Delta I/I_0$), which was defined as $\Delta I = (I_0 - I)$, illuminate a good linear relation with the logarithm of NSE concentration ($\log C_{NSE}$) range from 0.1 ng mL^{-1} to 1000 ng mL^{-1}, the detection limit is 0.05 ngmL^{-1} (S/N = 3). The regression equation was $\Delta I/I_0 = 0.1312 \log C_{NSE} + 0.2189$ (ng mL^{-1}, $R^2 = 0.9986$). Where I_0 and I were the photocurrents of the anti-NSE/DA/TiO_2/FTO electrode based immunosensor before (I_0) and after (I) immunoreactions with NSE (Fig. 7B), respectively. To further illustrate the excellent properties of the developed immunosensor, the results were compared with other immunoassay in Table S1 (Supporting Information). It was worth mentioning that the as-obtained biosensor reveals both a wider linear range and a lower detection limit. Furthermore, it indicates that, by combined with the specificity of immunoreactions and the sensitivity of PEC, this proposed PEC immunosensing strategy may provide a potential application for the NSE in the disease surveillance, therapy process, and early diagnosis.

Real sample analysis

The feasibility of this as-obtained immunosensor was investigated on the determination of NSE in clinical human serum samples. The serum samples were diluted by PBS solution. The comparison results were listed in Table 1. The results indicated that this proposed method could detect NSE in real samples with a wide concentration range of 0.47 ng mL^{-1}~87.21 ng mL^{-1}, and good recoveries varied in the range of 96.7%–105.5% (RSD: 2.0–6.4%). Therefore, it also demonstrated that the anti-NSE/DA/TiO_2/FTO based immunosensor had good practicability and sensitivity for the

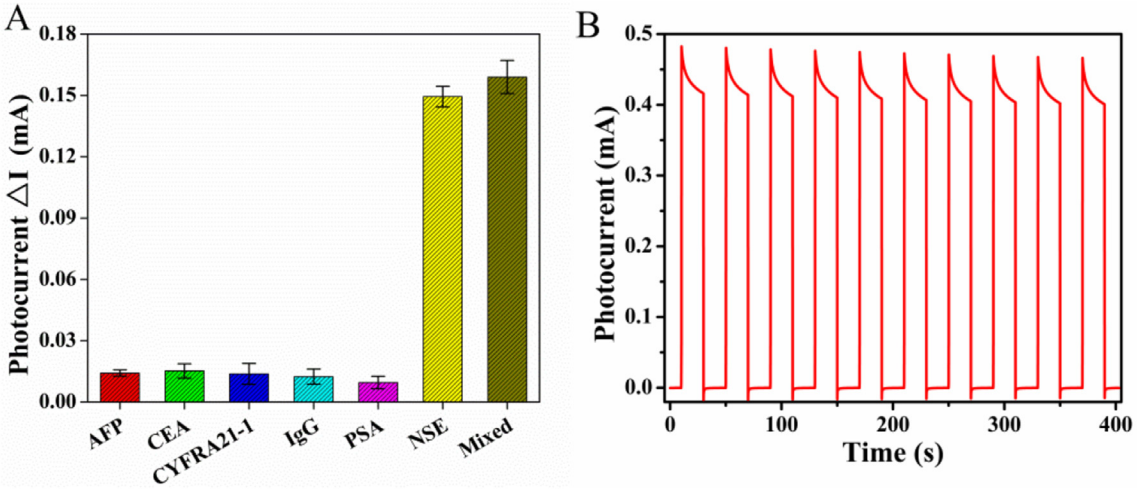

Fig. 6. (A) The selectivity of the proposed PEC immunoassay. (B) The stability of the as-obtained immunosensor in 0.1 M PBS (pH = 7.4) with light on and off 10 times.

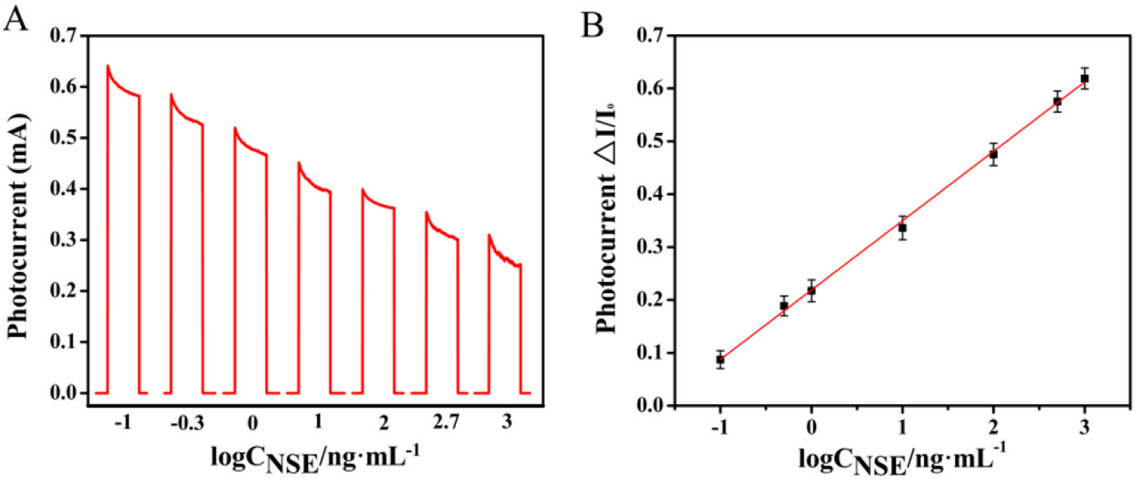

Fig. 7. Photocurrent responses (A) and corresponding calibration curve (B) of BSA/anti-NSE/DA/TiO_2/FTO electrode in the presence of different concentrations of NSE, which were measured in 0.1 M PBS (pH = 7.4).

Table 1
Determination of NSE in clinical serum samples by the proposed methods.

Sample	NSE concentration (ng/ml)			Recovery (%)	RSD (%, n = 3)
	Before addition	Added	After addition		
1	0.47	0.5	0.95	97.9	4.8
2	2.16	2.0	4.39	105.5	5.1
3	7.52	8.0	15.01	96.7	3.5
4	21.46	20.0	40.17	96.9	2.0
5	87.21	100.0	189.74	101.4	6.4

detection of NSE in clinical serum samples.

Conclusion

In short, 3D hyperbranched TiO_2 nanorod arrays were applied in the fabrication of PEC biosensor for the first time. A new signal amplification strategy was designed and realized by combining DA with TiO_2 to form charge transfer complex. The resulted PEC immunosensor for the detection of NSE possesses wide linear range, high sensitivity, good reproducibility, excellent selectivity and long-term stability. Additionally, the proposed immunosensor had an acceptable accuracy for the detection of NSE in human serum samples. The proposed method could be further developed not only for analyzing other biomarkers but also for the potential application in clinical diagnosis.

Acknowledgments

This research was financial supported by the Science and Technology Planning Project of Guangzhou (No. 2009Z2-D511) and Guangzhou Key Laboratory of Analytical Chemistry for Biomedicine (No. 201509010001), China.

Appendix A. Supplementary data

Supplementary data related to this article can be found at http://dx.doi.org/10.1016/j.ab.2017.05.025.

References

[1] H. Kitano, Systems biology: a brief overview, Science 295 (2002) 1662–1664.
[2] P.R. Srinivas, B.S. Kramer, S. Srivastava, Trends in biomarker research for cancer detection, Lancet. Oncol. 2 (2001) 698–704.
[3] P.J. Marangos, D.E. Schmechel, Neuron specific enolase, a clinically useful marker for neurons and neuroendocrine cells, Annu. Rev. Neurosci. 10 (1987) 269–295.
[4] S.M. Wu, L.F. Liu, G. Li, F.X. Jing, H.J. Mao, Q.H. Jin, W.Y. Zhai, H.F. Zhang, J.L. Zhao, C.P. Jia, Multiplexed detection of lung cancer biomarkers based on quantum dots and microbeads, Talanta 156 (2016) 48–54.
[5] V. Medina-Hernandez, J. Ramos-Loyo, S. Luquin, L.F.C. Sanchez, J. Garcia-Estrada, A. Navarro-Ruiz, Increased lipid peroxidation and neuron specific enolase in treatment refractory schizophrenics, J. Psychiatr. Res. 41 (2007) 652–658.
[6] C.S. Li, B.C. Cheng, W. Ge, J.F. Gao, Clinical value of CYFRA21-1, NSE, CA15-3, CA19-9 and CA125 assay in the elderly patients with pleural effusions, Int. J. Clin. Pract. 61 (2007) 444–448.
[7] B. Wang, Y.J. He, Y.X. Tian, R.N. Yang, Y.R. Zhu, H. Qiu, Clinical utility of haptoglobin in combination with CEA, NSE and CYFRA21-1 for diagnosis of lung cancer, Asian Pac. J. Cancer P 15 (2014) 9611–9614.
[8] X.H. Fu, K. Xu, X.R. Feng, Synthesis of sunflower-like gold nanostructures and their application in electrochemical immunoassays using the nanogold-triggered hydrogen evolution reaction, Anal. Methods 8 (2016) 958–961.
[9] G.L. Wang, P.P. Yu, J.J. Xu, H.Y. Chen, A label-free photoelectrochemical immunosensor based on water-soluble CdS quantum dots, J. Phys. Chem. C 113 (2009) 11142–11148.
[10] S. Corezzi, L. Urbanelli, P. Cloetens, C. Emiliani, L. Helfen, S. Bohic, F. Elisei, D. Fioretto, Synchrotron-based X-ray fluorescence imaging of human cells labeled with CdSe quantum dots, Anal. Biochem. 388 (2009) 33–39.
[11] K. Ghanbari, N. Hajheidari, ZnO-Cu_xO/polypyrrole nanocomposite modified electrode for simultaneous determination of ascorbic acid, dopamine, and uric acid, Anal. Biochem. 473 (2015) 53–62.
[12] Y.R. An, Sirtuin 1 evaluation with a novel immunoassay approach based on TiO_2-Au label and hyperbranched polymer hybrid, Anal. Biochem. 507 (2016) 58–65.
[13] W. Lu, G. Wang, Y. Jin, X. Yao, J.Q. Hu, J.H. Li, Label-free photoelectrochemical strategy for hairpin DNA hybridization detection on titanium dioxide electrode, Appl. Phys. Lett. 89 (2006).
[14] T.T. Tran .T, J.Z. Li, H. Feng, J. Cai, L.J. Yuan, N.Y. Wang, Q.Y. Cai, Molecularly imprinted polymer modified TiO_2 nanotube arrays for photoelectrochemical determination of perfluorooctane sulfonate (PFOS), Sens. Actuat. B-Chem. 190 (2014) 745–751.
[15] L.Q. Yu, Y.P. Zhang, Q.Q. Zhi, Q.Q. Wang, F.S. Gittleson, J.Y. Li, A.D. Taylor, Enhanced photoelectrochemical and sensing performance of novel TiO_2 arrays to H_2O_2 detection, Sens. Actuat. B-Chem. 211 (2015) 111–115.
[16] H. Tokudome, Y. Yamada, S. Sonezaki, H. Ishikawa, M. Bekki, K. Kanehira,

M. Miyauchi, Photoelectrochemical deoxyribonucleic acid sensing on a nanostructured TiO_2 electrode, Appl. Phys. Lett. 87 (2005).
[17] D. Chen, H. Zhang, X. Li, J.H. Li, Biofunctional titania nanotubes for visible-light-activated photoelectrochemical biosensing, Anal. Chem. 82 (2010) 2253–2261.
[18] H.B. Li, J. Li, Q. Xu, X.Y. Hu, Poly(3-hexylthiophene)/TiO_2nanoparticle-functionalized electrodes for visible light and low potential photoelectrochemical sensing of organophosphorus pesticide chlopyrifos, Anal. Chem. 83 (2011) 9681–9686.
[19] Q. Kang, L.X. Yang, Y.F. Chen, S.L. Luo, L.F. Wen, Q.Y. Cai, S.Z. Yao, Photoelectrochemical detection of pentachlorophenol with a multiple hybrid $CdSe_xTe_{1-x}/TiO_2$nanotube structure-based label-free immunosensor, Anal. Chem. 82 (2010) 9749–9754.
[20] H. Li, J.L. Lu, Y. Wang, F.Y. Yi, X.D. Guo, An ultrasensitive immunosensor for the detection of carcinoembryonic antigens utilizing a Nb-doped titanium dioxide nanocomposite film, Nano 10 (2015).
[21] H. Li, X.W. Huang, J.L. Lu, F. Sun, F.Y. Yi, Y. Wang, Y.W. Tang, A novel glucose biosensor fabricated with electroactive $Nb_{0.95}Ti_{0.95}O_4$nano-composite film, Int. J. Electrochem. S. 7 (2012) 9354–9365.
[22] J.J. Tao, Z.Z. Gong, G. Yao, Y.L. Cheng, M. Zhang, J.G. Lv, S.W. Shi, G. He, X.S. Chen, Z.Q. Sun, Enhanced photocatalytic and photoelectrochemical properties of TiO_2 nanorod arrays sensitized with CdS nanoplates, Ceram. Int. 42 (2016) 11716–11723.
[23] Y.L. Li, S.P. Zhang, H. Dai, Z.S. Hong, Y.Y. Lin, An enzyme-free photoelectrochemical sensing of concanavalin a based on graphene-supported TiO_2 mesocrystal, Sens. Actuat. B-Chem. 232 (2016) 226–233.
[24] M. Zeng, X.G. Peng, J.J. Liao, G.Z. Wang, Y.F. Li, J.B. Li, Y. Qin, J.S. Wilson, A.M. Song, S.W. Lin, Enhanced photoelectrochemical performance of quantum dot-sensitized TiO_2 nanotube arrays with Al_2O_3 overcoating by atomic layer deposition, Phys. Chem. Chem. Phys. 18 (2016) 17404–17413.
[25] Z. Pan, Y. Qiu, J. Yang, M. Liu, L. Zhou, Y. Xu, L. Sheng, X. Zhao, Y. Zhang, Synthesis of three-dimensional hyperbranched TiO_2nanowire arrays with significantly enhanced photoelectrochemical hydrogen production, J. Mater. Chem. A 3 (2015) 4004–4009.
[26] W.Q. Wu, B.X. Lei, H.S. Rao, Y.F. Xu, Y.F. Wang, C.Y. Su, D.B. Kuang, Hydrothermal fabrication of hierarchically anatase TiO_2 nanowire arrays on FTO glass for dye-sensitized solar cells, Sci. Rep. 3 (2013) 1352.
[27] W.Q. Wu, H.S. Rao, H.L. Feng, H.Y. Chen, D.B. Kuang, C.Y. Su, A family of vertically aligned nanowires with smooth, hierarchical and hyperbranched architectures for efficient energy conversion, Nano Energy 9 (2014) 15–24.
[28] W.Q. Wu, H.L. Feng, H.S. Rao, Y.F. Xu, D.B. Kuang, C.Y. Su, Maximizing omnidirectional light harvesting in metal oxide hyperbranched array architectures, Nat. Commun. 5 (2014) 3968.
[29] T. Rajh, L.X. Chen, K. Lukas, T. Liu, M.C. Thurnauer, D.M. Tiede, Surface restructuring of nanoparticles: an efficient route for ligand-metal oxide crosstalk, J. Phys. Chem. B 106 (2002) 10543–10552.
[30] W.W. Zhao, Z.Y. Ma, J.J. Xu, H.Y. Chen, In situ modification of a semiconductor surface by an enzymatic process: a general strategy for photoelectrochemical bioanalysis, Anal. Chem. 85 (2013) 8503–8506.
[31] G.L. Wang, J.J. Xu, H.Y. Chen, S.Z. Fu, Label-free photoelectrochemical immunoassay for alpha-fetoprotein detection based on TiO_2/CdS hybrid, Biosens. Bioelectron. 25 (2009) 791–796.
[32] Y.J. Li, M.J. Ma, G. Yin, Y. Kong, J.J. Zhu, Phthalocyanine-sensitized graphene-CdS nanocomposites: an enhanced photoelectrochemical immunosensing platform, Chemistry 19 (2013) 4496–4505.